Supplementary Material (SM) for:

Interaction dimensionality scales up to generate bimodal consumer-resource size-ratio distributions in ecological communities

Samraat Pawar[1,*], Anthony I. Dell[2,3], Tianyun Lin[4], Daniel J. Wieczynski[4], Van M. Savage[4,5]

[1]Department of Life Sciences, Imperial College London, Silwood Park, Ascot, Berkshire, United Kingdom
[2]National Great Rivers Research and Education Center (NGRREC), East Alton, Illinois, USA
[3]Department of Biology, Washington University in St. Louis, St. Louis, Missouri, USA
[4]Department of Ecology and Evolutionary Biology, University of California, Los Angeles, Los Angeles, California, USA
[5]Santa Fe Institute, Santa Fe, New Mexico, USA.

Appendix 1: Size-dependence of attack success

Following encounter beyond an intermediate size ratio (k_{pk}) of maximal attack success—as resources become much too large for the consumer to pursue, subjugate and ingest—attack success probability (A), and therefore also consumption rate (and thus, effectively, search rate), should decline. Previous empirical studies suggest this decline in A is a power-law (Persson et al, 1998; Aljetlawi et al., 2004; Brose et al., 2008; Vucic-Pestic et al., 2010). To evaluate the generality of this pattern and to obtain estimates of range of values the scaling exponent can take, we compiled from the literature a dataset of laboratory studies that measure consumption rate (main text Equation (1); cf. main text Equation (5)) at different size ratios ($k = m_R/m_C$) for the same consumer-resource pair. Methodology for extracting these data is described in Pawar et al. (2012). We found 11 laboratory studies, which yielded 16 responses of consumption rate with respect to body-size size ratio, between 25 distinct consumer-resource pairs (including different life stages of the same species) (Fig. S1; Table S2). When functional responses were measured, we recorded consumption rates at every reported resource density. We excluded studies with less than four distinct size ratio values, and where multiple consumer or resource species were used simultaneously.

Consumption rate estimates at each unique size ratio were converted to the product of per-capita search rate and attack success probability, aA, by dividing out resource biomass density from main text Equation (1) (with $f = 1$ for the searching phase of the interaction). Note that this assumes, as does the attack success model (main text Equation (4)), that per-capita attack success probability is independent of resource density. For functional responses, we used consumption rate at the lowest resource density (linear part of the response) to calculate search rate. Multiple consumer-resource pairs with identical taxonomic identities, life stages, and body masses were considered pseudoreplicates.

Table S1. Criteria used to assign dimensionality (***D***) and foraging strategy to interactions. The habitat of an interaction is defined by the space in which the resource is typically captured. Dimensionality is mainly determined by the movement space of the resource. For example, a pelican catching a fish at the water surface is classified as a 2*D* aquatic interaction.

Consumer foraging movement and location in habitat	Resource movement and location in habitat	*D*	Foraging strategy
Flying in air or swimming in water column	Flying in air or swimming in water column	3*D*	Active capture
Moving on land or water bottom/surface	Flying in air or swimming in water column	3*D*	Active capture
Flying in air or swimming in water column	Moving on land or water bottom/surface	2*D*	Active capture

Flying in air or swimming in water column	Moving on land or water bottom/surface	2*D*	Active capture
Moving on land or water bottom/surface	Moving on land or water bottom/surface	2*D*	Active capture
Sessile on land or water bottom/surface or suspended in water column	Flying in air or swimming in water column	3*D*	Sit-and-wait
Sessile on land or water bottom/surface	Moving on land or water bottom/surface	2*D*	Sit-and-wait
Actively swimming in water column	Sessile or passive in water column	3*D*	Grazing
Flying in air or swimming in water column	Sessile on land or water bottom/surface	2*D*	Grazing
Moving on land or water bottom/surface	Sessile on land or on water bottom/surface	2*D*	Grazing

Each consumer-resource pair was assigned an interaction dimensionality based on consumer search space (Table S1, main text Fig. 1; also see Pawar et al. (2012)). If a consumer searches (by flying, swimming, or sitting-and-waiting) for resources on habitat surfaces (e.g., water surface, benthos, grassland), the interaction is two dimensional (2*D*), and if it searches habitat volume, the interaction is three dimensional (3*D*). As discussed in the main text, this apparently simple classification of interaction dimensionality is consistent with detection regions typically having Euclidean/integer dimensionality. In addition, dimensionality was assigned at the level of life stage (provided a consumer-resource pair was resolved to that level), to minimize the confounding effect of ontogenetic diet shifts and associated changes in foraging dimensionality and strategy.

Species average body masses were obtained from the original study when reported or estimated using methods previously described (Dell et al., 2011; Dell et al., 2013). For each consumption-rate dataset we recorded the size ratio (k_{pk}) at which search rate aA peaked. An alternative approach would be to estimate k_{pk} by fitting a unimodal function, but most of the data lack sufficient measurements on both sides of the peak to allow reliable parameter estimates. To evaluate the relationship between aA and k, we first split each dataset (response) into rising (all aA values $\leq k_{pk}$) and falling (all aA values $\geq k_{pk}$) parts. We then performed separate ordinary least squares (OLS) regression in rising and falling parts of $\log_{10}$ consumer mass-normalized search rate ($aA/m_C^{0.7}$ in 2*D* and $aA/m_C^{1.05}$ in 3*D*; approximately the exponents for scaling of size-scaling of search rate reported by Pawar et al (2012)) vs. $\log_{10}k$. This consumer mass correction isolates the effect on consumption rate of size-ratio from that of consumer mass. This yielded estimates of exponents for the rising and falling parts (α and γ respectively) for each dataset. We did not attempt to estimate either exponent if the number of data points in the respective rising or falling part of the series was less than four. To evaluate whether a power-law (with exponent γ) adequately quantifies decline above k_{pk}, along with standard goodness-of fit statistics, we examined regression residuals for systematic deviations by fitting a quadratic model. For example, if an exponential or linear decline was more appropriate than a power-law, the residuals would show significant concave downward curvature and be best fit by a quadratic regression model. In contrast, lack of systematic deviation would be indicated by a straight line with slope ~ 0 being a better fit.

Fig. S1 and Table S2 show the results of our meta-analyses. Although few studies cover sufficient range of size-ratios to capture a full unimodal response of search rate aA (Fig. S1), we find that a power-law (main text Equation (4)) is an acceptable model for decline in aA at high ratios, with the scaling exponent γ ranging between ~1 to 4. We did not find significant quadratic curvature deviations of the residuals in any of the responses. Ideally, these data should also allow comparison of empirical estimates of the rising part of the k function (exponent α in Fig. S1 and Table S2) with the exponents expected from main text Equation (3) and Equations (S13)–(S15) (the exponents associated with k in these equations). However, in most datasets, portions of the unimodal function above and below the peak are too poorly resoved to provide reliable estimates of the scaling exponents. Only three datasets allowed calculation of both α and γ exponents of the unimodal relationship between aA and k, while two datasets allowed neither. Nevertheless, we note that α tends to be steeper in 3*D* than 2*D* (Fig. S1 and Table S2), consistent with our theory (main text Equation

(3) and Equations (S13)–(S15)). Therefore, for our theoretical analysis we use a power function for A (with exponent γ; main text Equation (4)). We test the sensitivity of our results by varying γ (see Appendix 3), and by using an exponential instead of power-law form of A (Appendix 3).

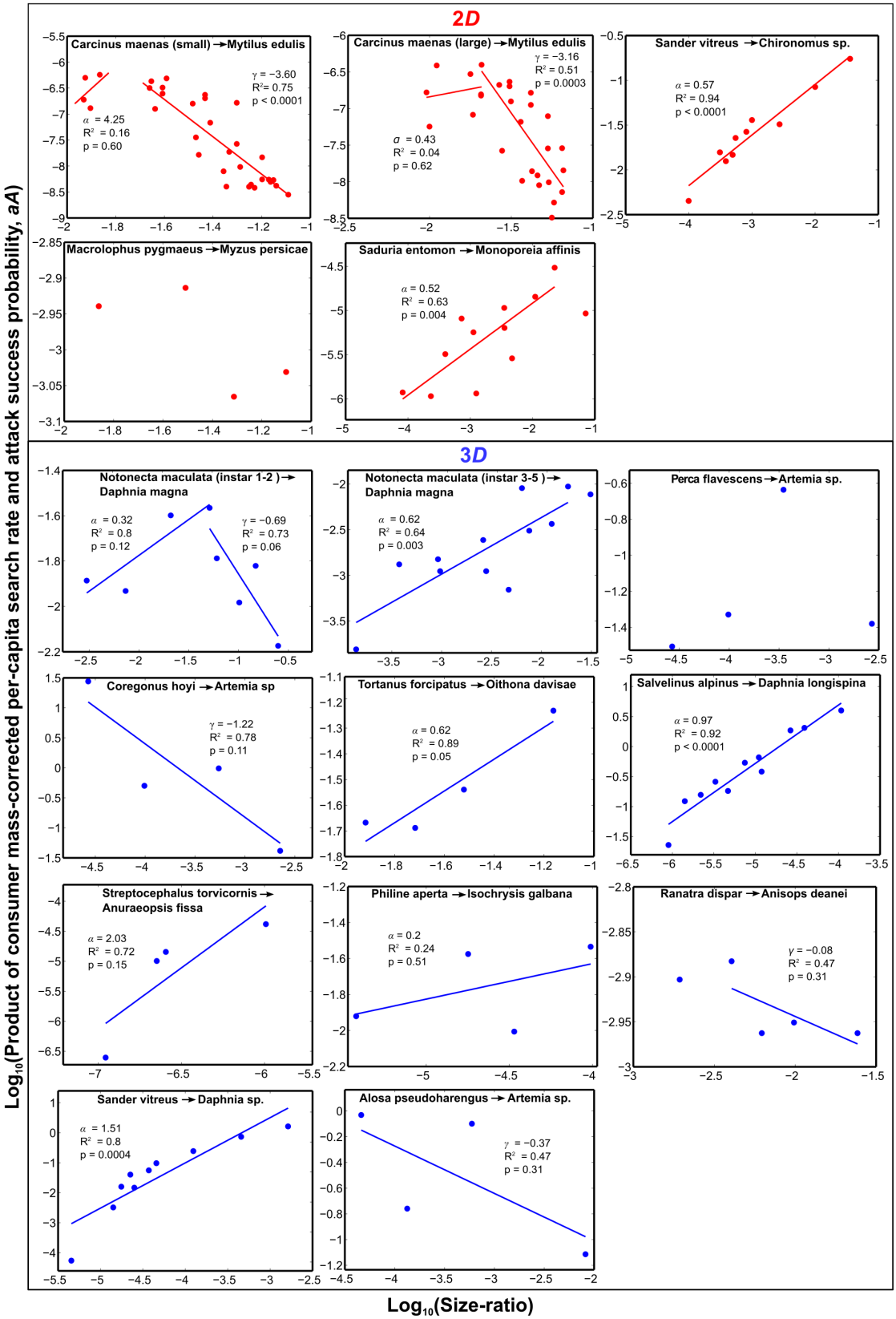
2D
Carcinus maenas (small) → Mytilus edulis
γ = −3.60
R² = 0.75
p < 0.0001
α = 4.25
R² = 0.16
p = 0.60
Carcinus maenas (large) → Mytilus edulis
γ = −3.16
R² = 0.51
p = 0.0003
α = 0.43
R² = 0.04
p = 0.62
Sander vitreus → Chironomus sp.
α = 0.57
R² = 0.94
p < 0.0001
Macrolophus pygmaeus → Myzus persicae
Saduria entomon → Monoporeia affinis
α = 0.52
R² = 0.63
p = 0.004
3D
Notonecta maculata (instar 1-2) → Daphnia magna
α = 0.32
R² = 0.8
p = 0.12
γ = −0.69
R² = 0.73
p = 0.06
Notonecta maculata (instar 3-5) → Daphnia magna
α = 0.62
R² = 0.64
p = 0.003
Perca flavescens → Artemia sp.
Coregonus hoyi → Artemia sp
γ = −1.22
R² = 0.78
p = 0.11
Tortanus forcipatus → Oithona davisae
α = 0.62
R² = 0.89
p = 0.05
Salvelinus alpinus → Daphnia longispina
α = 0.97
R² = 0.92
p < 0.0001
Streptocephalus torvicornis → Anuraeopsis fissa
α = 2.03
R² = 0.72
p = 0.15
Philine aperta → Isochrysis galbana
α = 0.2
R² = 0.24
p = 0.51
Ranatra dispar → Anisops deanei
γ = −0.08
R² = 0.47
p = 0.31
Sander vitreus → Daphnia sp.
α = 1.51
R² = 0.8
p = 0.0004
Alosa pseudoharengus → Artemia sp.
γ = −0.37
R² = 0.47
p = 0.31
Log10(Product of consumer mass-corrected per-capita search rate and attack success probability, aA)
Log10(Size-ratio)

89

Figure S1. Relationship between consumer mass-corrected product of search rate and attack success probability (aA) and size-ratio (k). Each panel represents an experiment with a single consumer feeding on a single resource species across a range of size ratios k. The lines are OLS fits. We do not use major axis (MA) regression because our objective is to obtain the most accurate (not necessarily the least biased) prediction of search rate scaling (Warton et al., 2006). Using MA regression yields steeper exponents, but does not alter our results qualitatively. Further details of statistical analyses and data sources are in Table S2. Datasets with insufficient data points on either side of maximum aA do not have fitted lines.

Table S2. Scaling of consumer mass-corrected product of search rate and attack success probability (aA) with consumer-resource size-ratio (k) across laboratory studies (cf. Fig. S1). Each interaction has been classified by dimensionality (D) and foraging strategy (For: A – active-capture, G – grazing, S – sit-and wait). k_{pk} denotes size-ratio at which aA peaks. The R^2 and F-statistic p-value of the respective OLS regression analysis to estimate α (rise in aA up to k_{pk}) and γ (fall in aA after k_{pk}) in each dataset is shown along with sample sizes (n (α) and n (γ) columns, respectively). Exponents with $p < 0.05$ and $R^2 \geq 0.5$ are flagged by "*".Values that could not be calculated due to lack of data are indicated by "-". Note that none of the responses for which sufficient data were available to characterize the falling part showed significant curvature (indicated by "NS").

Consumer → Resource	D	k_{pk}	For	n (α)	α ±95%CI	R^2	p-value	n (γ)	γ ±95%CI	R^2	p-value	Data source
Carcinus maenas (small) → *Mytilus edulis*	2	1.36×10^{-02}	G	4	4.25 ±29.5	0.16	NS	29	3.6* ±0.81	0.75	<0.0001	Walne & Dean, 1972
Carcinus maenas (large) → *Mytilus edulis*	2	2.08×10^{-02}	G	8	0.42 ±1.98	0.04	NS	21	3.2* ±1.4	0.51	<0.0001	Walne & Dean, 1972
Macrolophus pygmaeus → *Myzus persicae*	2	3.10×10^{-02}	G	-	-	-	-	-	-	-	-	Fantinou, 2009
Saduria entomon → *Monoporeia affinis*	2	2.26×10^{-02}	A	11	0.52* ±0.3	0.63	0.004	-	-	-	-	Aljetlawi et al., 2004
Sander vitreus → *Chironomus sp.*	2	3.58×10^{-02}	A	10	0.57* ±0.1	0.94	<0.0001	-	-	-	-	Galarowicz & Wahl, 2005
Alosa pseudoharengus → *Artemia sp.*	3	4.62×10^{-05}	A	-	-	-	-	4	0.37 ±1.2	0.47	NS	Miller et al., 1992
Coregonus hoyi → *Artemia sp.*	3	2.68×10^{-05}	A	-	-	-	-	4	1.2 ±1.9	0.78	NS	Miller et al., 1992
Notonecta maculata (instar 1-2) → *Daphnia magna*	3	5.12×10^{-02}	A	4	0.32 ±0.49	0.80	NS	5	0.69 ±0.77	0.73	NS	Gergs & Ratte, 2009
N. maculata (instar 3-5) → *Daphnia magna*	3	1.85×10^{-02}	A	11	0.62* ±0.35	0.64	0.003	-	-	-	-	Gergs & Ratte, 2009
Perca flavescens → *Artemia sp.*	3	3.51×10^{-04}	A	-	-	-	-	-	-	-	-	Miller et al., 1992
Philine aperta → *Isochrysis galbana*	3	9.75×10^{-05}	A	4	0.20 ±1.08	0.24	NS	-	-	-	-	Hansen & Ockelmann, 1991
Ranatra dispar → *Anisops deanei*	3	4.05×10^{-03}	S	-	-	-	-	4	0.08 ±0.25	0.47	NS	Bailey, 2010
Salvelinus alpinus → *Daphnia longispina*	3	1.08×10^{-04}	A	11	0.97* ±0.21	0.92	<0.0001	-	-	-	-	Jansen et al., 2003
Sander vitreus → *Daphnia sp.*	3	1.63×10^{-03}	A	10	1.5* ±0.61	0.80	<0.0001	-	-	-	-	Galarowicz & Wahl, 2005
Streptocephalus torvicornis → *Anuraeopsis fissa*	3	1.02×10^{-06}	A	4	2.03 ±3.89	0.71	NS	-	-	-	-	Dierckens et al., 1995
Tortanus forcipatus → *Oithona davisae*	3	6.88×10^{-02}	A	4	0.62 ±0.65	0.89	0.05	-	-	-	-	Uye & Kayano 1994

Appendix 2: Theoretically feasible size-ratios for consumer-resource coexistence and population stability

Here, to compare and contrast with the theoretically feasible size-ratios predicted by our model for consumer population energetics, we consider the feasibility of size-ratios from a population dynamical perspective. For this, we use a general Rosenzweig-Macarthur type model for changes in consumer-resource biomass densities C (= $m_C x_C$) and R (= $m_R x_R$) respectively (Weitz and Levin, 2006; Dell et al., 2013):

$$\begin{aligned} \frac{dR}{dt} &= rR\left(1-\frac{R}{K}\right)-\frac{a'AR}{1+aAhR}C \\ \frac{dC}{dt} &= -zC+e\frac{a'AR}{1+aAhR}C \end{aligned} \tag{S1}$$

Here, r is the resource's intrinsic biomass production rate (1/time), z the consumer's biomass loss rate (including mortality) (1/time), a' is consumer-mass specific search rate ($a'=a/m_C$, because Equations (S1) are in biomass units; cf. main text Equation (3)) and e is conversion efficiency of resource biomass into consumer biomass (a proportion). K is resource carrying capacity (mass × area^{-1} or volume^{-1}) — the maximum biomass density achieved by the resource in the absence of consumers. That is, K equals resource mass m_R multiplied by its carrying capacity in terms of number density. Equilibrium biomass densities (kg × m^{-2} or kg × m^{-3}) for the consumer-resource system with Type II functional response (Equations (S1)) are

$$\begin{aligned} \hat{R} &= \frac{z}{a'A(e-zh)} \\ \hat{C} &= \frac{er(Ka'A(e-zh)-z)}{K(a'A)^2(e-zh)^2} \end{aligned} \tag{S5}$$

Coexistence means that the consumer maintains positive equilibrium biomass ($\hat{C}>0$), which in turn implies $K > z/(a'A(e-zh))$. In other words, the resource growing to its carrying capacity $K = z/(a'A(e-zh))$ is necessarily only possible when the consumer has gone extinct (no coexistence). The biological insight from this inequality is that coexistence is only possible if resource carrying capacity is sufficiently large to sustain consumers even if they have high mortality, low search rate, low efficiency, or high handling times. Here again, as we did for the energetic model (see main text), we assume $h = 0$ (Type I $f(R)$) to obtain an exact solution, which simplifies the coexistence condition to $K > z/ea'A$.

Now we can again substitute the scaling of the species interaction parameters (main text Equations (3), (4), (6)), along with scaling of the additional parameters r, z, and K. For the latter three, we use the well-established relationships (Yodzis and Innes, 1992; Weitz and Levin, 2006; Pawar et al., 2012)

$$r = r_0 m_R^{\beta-1} \tag{S2}$$

$$z = B_0 m_C^{\beta-1} \tag{S3}$$

$$K = x_0 m_R^{1-\beta_x} \tag{S4}$$

where the constants r_0, B_0, and x_0 include effects of temperature (Brown et al 2005; Dell et al., 2014; Pawar et al., 2015). Of these, note that we assume K scales like resource biomass density does in main text Equation (9). This is independent of interaction dimensionality because K represents maximal biomass density that the resource can achieve in absence of consumers (so dimensionality should play no part in this) (Savage et al., 2004; Pawar et al., 2012). Also, following empirical evidence (Peters, 1986; Pawar et

al., 2012), baseline carrying capacity (x_0) is assumed to be about two orders of magnitude higher in 3*D* than 2*D* (Table S3). Note that although biomass density *K* is expressed in per-volume units in 3*D* and per-area units in 2*D* (Table S3), what matters is that a greater amount of resource biomass can be packed into a 3*D* space. Substituting all these scaling Equations ((main text Equations (3), (4), (6), and (S2)–(S4)) into this coexistence condition, keeping in mind that $a = a'/m_C$, and rearranging so that m_R lies on the left hand size of the inequality, gives

$$m_R > m_0 \left(m_C^{\beta - p_d(D-1) - p_v} (1 + k^\gamma)^{-1} \right)^{\frac{1}{1 + p_d(D-1) - \beta}}, \tag{S6}$$

where $m_0 = (B_0/ea_0x_0)^{\frac{1}{1+p_d(D-1)-\beta}}$. Furthermore, substituting actual values for the exponents (Table S3), we get

$$\begin{aligned} m_R &> m_0 m_C^{0.64} (1 + k^\gamma)^{-2.22} \text{ in } 2D, \text{and} \\ m_R &> m_0 m_C^{0.14} (1 + k^\gamma)^{-1.54} \text{ in } 3D, \end{aligned} \tag{S7}$$

where $m_0 = (B_0/ea_0\ x_0)^{2.22}$ in 2*D* and $(B_0/ea_0x_0)^{1.54}$ in 3*D*. In Appendix 3, we show that the scaling of coexistence in Equation (S6) is qualitatively the same for Type II and III functional responses. The smaller m_C and *k* exponents for 3*D* in Equation (S7) imply that size constraints weaken as dimensionality increases. Therefore, relative to 2*D*, a much wider range of resource sizes become feasible for larger 3*D* consumers (main text Fig. 2). Conversely, 3*D* foraging allows an increased range of consumer sizes on a resource of given size because for a given size-ratio, larger consumers enjoy a greater mass-specific search rate in 3*D* than in 2*D* ($a' = a/m_C \propto m_C^{0.04}$in 3*D* but $m_C^{-0.34}$in 2*D*, from parameterized main text Equation (3)). Furthermore, within either 2*D* or 3*D,* feasible size-ratios for coexistence are predicted to be constrained by baseline biomass carrying capacity (K_0) (main text Fig. 2). Numerical values for all scaling parameters of Equation (S6) are summarized in Table S3.

Furthermore, dividing Equations (S5) by the respective body masses gives numerical abundances of consumer ($\hat{x}_C = \hat{C}/m_C$) and resource ($\hat{x}_R = \hat{R}/m_R$). Substituting the scaling of parameters (Table S3) into these equations and again assuming $h = 0$ gives the abundance scaling within the feasible coexistence region:

$$\begin{aligned} \hat{x}_R &= R_0 m_C^{-0.91} k^{-1.2} (1 + k^\gamma) \text{ in } 2D, \text{and} \\ \hat{x}_R &= R_0 m_C^{-1.31} k^{-1.4} (1 + k^\gamma) \text{ in } 3D \end{aligned} \tag{S8}$$

and

$$\begin{aligned} \hat{x}_C &= C_0 m_C^{-0.91} k^{-0.45} (1 + k^\gamma) \left(ea_0 K_0 - B_0 m_C^{-0.16} k^{-0.45} (1 + k^\gamma) \right) \text{ in } 2D, \text{and} \\ \hat{x}_C &= C_0 m_C^{-1.31} k^{-0.65} (1 + k^\gamma) \left(ea_0 K_0 - B_0 m_C^{-0.56} k^{-0.65} (1 + k^\gamma) \right) \text{ in } 3D \end{aligned} \tag{S9}$$

where $R_0 = B_0/ea_0$ and $C_0 = r_0/ea_0^2x_0$. Equations (S8) and (S9) predict qualitatively similar (negative) scaling of consumer and resource equilibrium abundances, which also hold for Type II functional responses (Fig. S2). Because resources are consumed most rapidly at intermediate size-ratios (along the $k = 1$ line in main text Fig. 2), for fixed consumer [resource] size, consumers [resources] reach highest [lowest] numbers at extreme size-ratios irrespective of dimensionality because of the unimodal size-ratio dependence of per-capita consumption rate (main text Equation (5)). This is also obvious in Equations (S8) and (S9). The initial power-law decrease in abundance with size-ratio (negative exponents on *k*) is balanced and then reversed by inverse $g(k) = 1+k^\gamma$ at very high size-ratios ($m_R \gg m_C$; main text Fig. 2).

Stability

To study local asymptotic stability to small perturbations around these equilibrium abundances (Equations (S8)–(S9)), we calculate size scaling of the two eigenvalues of the system's Jacobian matrix (Appendix 2). For this, we begin with the Jacobian matrix for the system:

$$\hat{\jmath} = \begin{bmatrix} -\frac{rz(e + h(z - eKa'A) + Kzh^2a'A)}{eKa'A(e - zh)} & -\frac{z}{e} \\ r(e - \frac{z}{Ka'A} - zh) & 0 \end{bmatrix} \quad \text{(S10)}$$

Where $a' \equiv a/m_C$ as before. The two eigenvalues of $\hat{\jmath}$ are,

$$\lambda(\hat{J})_{1,2} = \frac{rz(ehKa' - h^2Kza' - e - hz) \pm \sqrt{rz(rz(e - ehKa' + hz(1 + hKa'))^2 - 4eK(e - hz)^2a(eKa' - z(1 + hKa')))}}{2eKa'(e - hz)} \quad \text{(S11)}$$

These eigenvalues, which may consist of both real and imaginary (if the term under the square-root is negative) parts, determine behavior of the two populations following small perturbations around the equilibrium. Given Equation (S11), four scenarios are possible:

(i) both eigenvalues are real and negative ⇒ after perturbation, populations converge on the equilibrium exponentially without cycles (Fixed point)
(ii) both eigenvalues have imaginary and negative real parts ⇒ after perturbation, populations converge on the equilibrium with cycles (Transient cycles)
(iii) both eigenvalues have conjugate imaginary and positive real parts ⇒ after perturbation, populations diverge from the equilibrium with cycles (Persistent cycles)
(iv) One or both eigenvalues has a positive real part and neither has an imaginary part ⇒ equilibrium is unstable (Extinction)

We can characterize these scenarios in terms of consumer-resource body size ratios by substituting the scaling of parameters (see main text) into Equation (S11). The results (main text Fig. 2) show that within feasible size combinations, a larger range of size-ratios lead to persistent cycles in 3*D* than in 2*D*. As $h \rightarrow 0$ (→Type I functional response) we get,

$$\lambda(\hat{J})_{1,2} = \frac{-rz \pm \sqrt{rz(rz - 4eKa'(eKa' - z))}}{2eKa'} \quad \text{(S12)}$$

Now, the real part of both eigenvalues can are always negative, and therefore the inner regions of unstable persistent cycles in the consumer-resource size plane (main text Fig. 2) are replaced by transient cycles. Thus, consistent with consumer-resource theory, as $h \rightarrow 0$ and the functional response becomes Type I, regions of persistent cycles are replaced by transient cycles (main text Fig. 2).

Appendix 3: Model robustness

Here we consider the robustness of our theoretical results to variation in the scaling relationships used to parameterize the consumer-resource model. Ranges of numerical values for these scaling model parameters are summarized in Table S3. Overall, our results are qualitatively robust to variation in model predictions for these ranges of parameter values.

Table S3. Numerical values for the parameters in the energetic feasibility (main text Equations (1)–(7)) and consumer-resource dynamics models (Equations (S1)). The upper limit of h_0 is approximately the value obtained by Pawar et al. (2012) from a meta-analysis of empircal data on handling times. The lower and upper limits for β_h are based on scaling exponents of resting and active metabolic rates, respectively.

Parameter	Description	Parameter values	Units	Source
β	Exponent for scaling of metabolic rate	0.75 – 0.8	-	Peters, 1986; Brown et al., 2004; Savage et al., 2004; Nagy 2005
β_x	Exponent for scaling of numerical abundance	0.75	-	Peters, 1986; Brown et al., 2004
β_h	Exponent for scaling of handling time with body mass	0.75 – 1	-	Pawar et al., 2012
p_v	Exponent of velocity scaling with body mass	0.26	-	Pawar et al., 2012
p_d	Exponent of detection distance scaling	0.2	-	Pawar et al., 2012
γ	Exponent for scaling of attack success probability	1 – 4	-	Pawar et al., 2012
B_0	Normalization constant for resting metabolic rate (consumer's intrinsic biomass loss rate)	1×10^{-6} – 1×10^{-9}	-	Peters, 1986; Brown et al., 2004; Nagy, 2005
r_0	Normalization constant for resource biomass production rate	1.71×10^{-9}	$kg^{1-\beta} \times s^{-1}$	Brown et al., 2004; Savage et al., 2004
x_0	Normalization constant for resource abundance (energetic feasibility model) or carrying capacity (consumer-resource model)	0.01 – 1 (2*D*), 3 – 300 (3*D*)	$kg^{\beta-1} \times m^{-2}$ (2*D*), $kg^{\beta-1} \times m^{-3}$ (3*D*)	Pawar et al., 2012
a_0	Normalization constant for search rate	$10^{-3.08}$ (2*D*), $10^{-1.77}$ (3*D*)	$m^2 \times s^{-1}$ (2*D*), $m^3 \times s^{-1}$ (3*D*)	Pawar et al., 2012
h_0	Normalization constant for handling time	0 – 10^4	$kg^{\beta-1} \times s$	Pawar et al., 2012
e	Conversion efficiency of resource to consumer biomass	0.3 – 0.75	-	Peters, 1986; Yodzis & Innes, 1992; Lang et al., 2017

Effect of functional response type

Here we show that our results for scaling of coexistence and abundance are robust even if we use Type II or Type III instead of Type I functional response. For this, instead of main text Equation (2), we use the generalized functional response (Vucic-Pestic et al., 2010), $f(R) = R^{q+1}/1 + haR^{q+1}$ and analyze the population dynamics model (Equations (S1)). This equation reduces to the Type II response when $q = 0$. Fig. (S2) shows that predicted coexistence regions with Type III (and therefore also II) change very little from Type I, the main difference being a minor reduction in coexistence regions, especially in 2*D*. In addition, regions of persistent cycles observed with Type II responses (main text Fig. 2) decrease when Type III responses are used (results not shown). For these results, we use $q = 0.5$, which is the approximate midpoint of the range reported by previous studies (Vucic-Pestic et al., 2010; Pawar et al., 2012). Increasing q will further decrease coexistence and cycling regions, while decreasing it to 0 (Type II $f(R)$) leads to the same coexistence region as for Type I (main text Fig. 2), but without persistent cycles. Thus, overall our main results about differences between 2*D* and 3*D* coexistence and population dynamics remain qualitatively the same, the main difference being that Type III responses slightly decrease feasible ranges of consumer-resource size combinations at small consumer sizes in 2*D*, and shrink regions of persistent

cycles in both 2*D* and 3*D*. Both effects are driven by the initial lag in consumption rate in Type III responses. The decrease in coexistence regions due to Type III is stronger in 2*D* because resource biomass densities decrease with size in 2*D* interactions, amplifying the effect of a lag in initial consumption rate for small consumers.

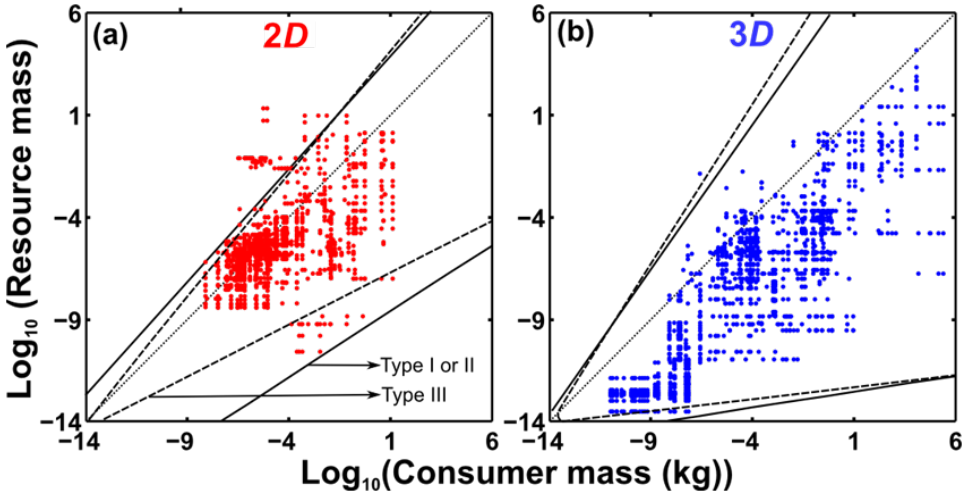

Figure S2. Differences in coexistence (abundances of both consumer and resource > 0) across all possible size combinations for Type I or II (bounded by solid lines) vs. Type III functional response (bounded by dashed lines). For Type III responses, we use q = 0.5 based on previous work (Pawar et al., 2012). Interactions from seven communities have been overlaid (1627 2*D* interactions and 1302 3*D* interactions). All other parameter settings are as in the main text figures.

Effect of foraging strategy

The scaling of per-capita search rate (main text Equation (3), which is for grazing) varies with foraging strategy (Pawar et al., 2012). Specifically, for grazing ($v_R \ll v_C$) (which we focus on in our main analyses and results)

$$a = a_0 m_C^{p_v+2p_d(D-1)} k^{p_d(D-1)} \quad \text{(S13)}$$

(same as main text Equation 3), for active-capture (both v_R & $v_C > 0$)

$$a = a_{0,D} m_C^{p_v+2(D-1)p_d} \sqrt{1+k^{2p_v}}\, k^{(D-1)p_d} \quad \text{(S14)}$$

and for sit-and-wait foraging ($v_R \gg v_C$)

$$a = a_{0,D} m_C^{p_v+2(D-1)p_d} k^{p_v+(D-1)p_d} \quad \text{(S15)}$$

with all parameters being same as those in main text Equation (3). Note that here the constant a_0 includes a *D* in the subscript, indicating that it increases with dimensionality (Pawar et al., 2012). We drop this part of the subscript in the main text for notational simplicity. Using empirically validated values of $p_v \sim 0.26$ and $p_d \sim 0.20$, Equations (S13)–(S15) predict that search rates should initially increase with *k* as a power-law, with exponents ranging from 0.20 (for grazing) to 0.46 (sit and wait) in 2*D* and 0.4 (grazing) to 0.66 (sit and wait) in 3*D*. There is very little overlap between these ranges, indicating that dimensionality is the main driver of variation in scaling, with foraging strategy having a secondary effect. Note that when the consumer is much larger than resource, the term under the square-root in Equation (S14) becomes very

small, and thus search rate in active-capture is well approximated by that of grazing ($a = a_{0,D} m_C^{p_v+2(D-1)p_d} k^{(D-1)p_d}$). Biologically, this means the consumer moves so much faster than resource that the velocity component of size-ratio scaling becomes insignificant. Because most available data are for grazers or active-capture consumers that are much larger than resources (Table S2 and Supplementary Data Table S4), we use the grazing model in all analyses in the paper.

To confirm robustness of our results to foraging strategy, we recalculate the coexistence regions (main text Fig. 2, which is for grazing) using Equations (S13)–(S15). The results are shown in Fig. S3a & b. Coexistence regions for active-capture (dotted lines) are almost identical to those for grazing (black lines), while those for sit-and-wait foraging are somewhat more restricted. However, our main results about the scaling of abundance (result not shown), location of population cycles on the size combination plane (result not shown), and differences between 2*D* and 3*D* regions (main text Fig. 2) remain qualitatively the same.

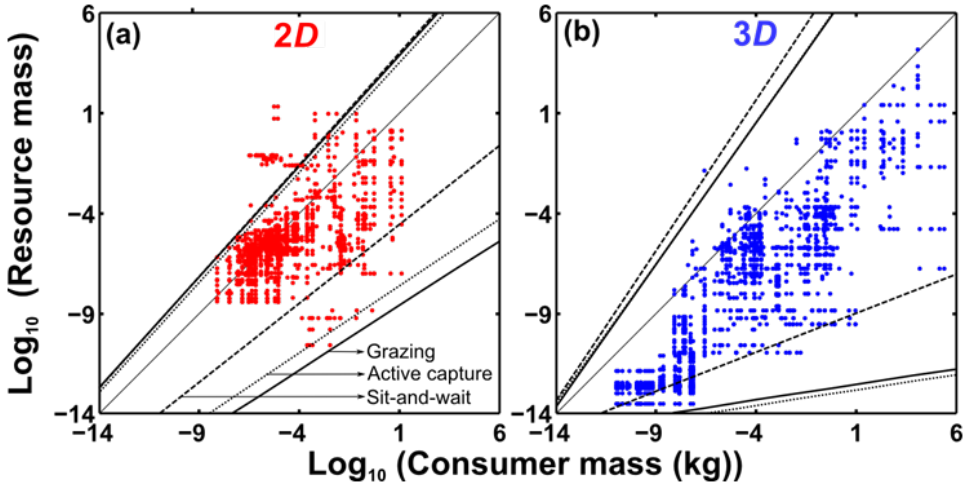

Figure S3. Differences in coexistence for grazing (within thick solid lines, same as regions in main text Fig. 2), active capture (Equation (S14); within dotted lines), and sit-and-wait foraging strategies (Equation (S15); within dashed lines). All parameter settings same as the ones used for main text Fig. 2.

Effect of variation in the attack success function

We now examine the effect of variation in the steepness of the power-law decline of attack success (A), which is governed by the exponent γ. To this end, we recalculate the coexistence regions with the approximate maximum and minimum values for γ determined from our empirical analyses (Fig. S1 and Table S2). The results are shown in Fig. S4a&b. As expected, decreasing strength of the power-law decline in attack success ($\gamma = 1$) weakens constraints on small consumer-large resource size combinations (where $k \gg 1$; Fig. S4), widening the feasible coexistence regions. Conversely, increasing strength of the decline in attack success ($\gamma = 4$) strengthens constraints on size-combinations where $k \gg 1$ and thus narrows feasible coexistence regions (Fig. S4). We also model an exponential decline (i.e., $g(k) = e^{-\gamma k}$ (Aljetlawi et al., 2004; Weitz and Levin, 2006; Brose et al., 2008) in attack success, which yields qualitatively similar results to the power-law (Fig. S4c&d). Thus, overall our main results about the difference between 2*D* and 3*D* coexistence and population dynamics remain qualitatively the same. We note that examining the effect of variation in γ is particularly important because it also incorporates the constraints of gape-limitation.

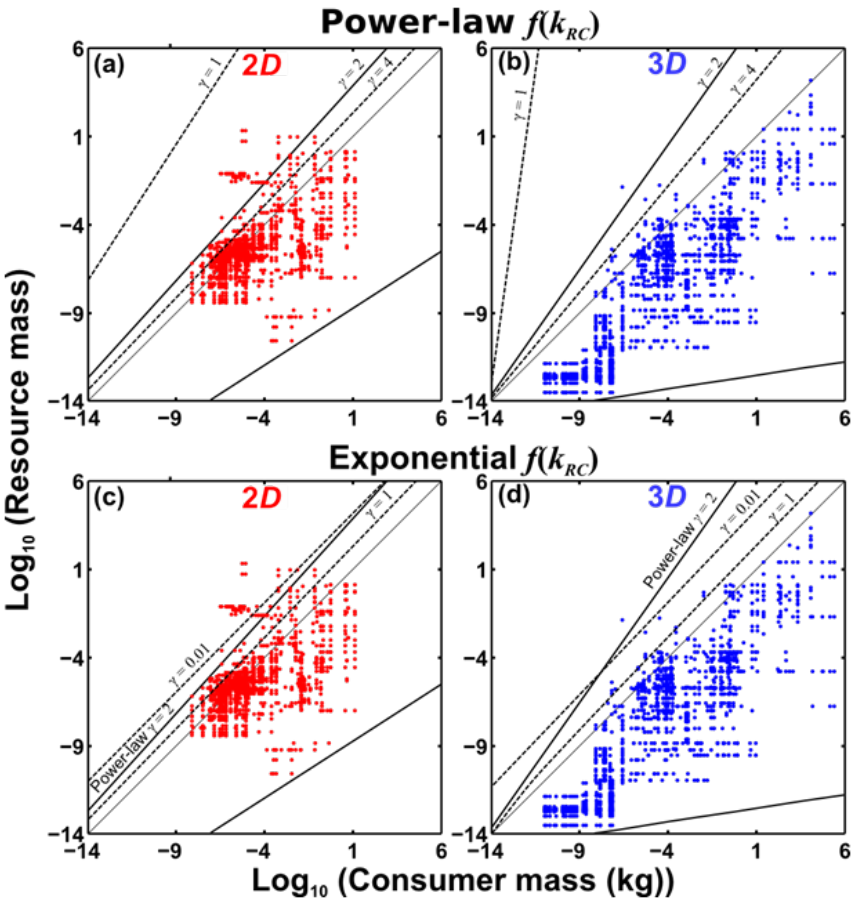

Figure S4. Sensitivity of coexistence to variation in scaling exponent γ (main text Equation (4)) (upper panel), and exponential instead of power-law decline in attack success probability (lower panel). In both sets of figures, results reported in the main text are bounded by thick black lines, while dashed lines show changes in the upper bounds due to variation in γ. All other parameter settings same as for main text Fig. 2.

Effect of monotonic versus unimodal attack success functions

We also compare two different models governing the shape of the attack success probability (ASP) function. Despite their unique mathematical forms, both ASP models generate numerically similar outputs for consumption rate. In the main analysis, we consider a monotonically decreasing function for ASP (main text Equation (4)), which still yields a unimodal consumption rate because search rate itself increases with respect to size ratio (main text Equation (3)). However, according to the results of Brose et al. (2008) and Vucic-Pestic et al., (2010), when resources are small enough that a consumer either cannot detect them or chooses to consume other resources that are easier to detect, ASP itself should be unimodal. Therefore, here we consider a Gaussian-like ASP function that includes a single optimal size ratio and declines in ASP for both small and large size ratios

$$\hat{A} = \exp\left[-\frac{\left(k - k_{\text{pk}}\right)^2}{2\sigma^2}\right] \tag{S16}$$

where k_{pk} is the mean (optimal) size-ratio, and σ^2 is the variance in ASP across size ratios.

To compare these two ASP models and study the sole effect of size-ratio on consumption rate, first we simplify main text Equation (5) by setting consumer mass to a constant ($m_C = 1$)

$$c = \frac{ASP \cdot a_0 k^{p_d(D-1)+1} x_R}{1 + a_0 k^{p_d(D-1)+1} \cdot ASP \cdot h_0} \tag{S17}$$

where ASP can equal either A (main text Equation (4)) or $\hat{A}$ as defined above. If we only consider the 2D case, we can set $p_d = 0.2$ (Table S3) and $D = 2$ and consumption rate can be rewritten as

$$c = \frac{x_R}{\frac{1}{a_0 \, ASP \cdot k^{1.2}} + h_0} \tag{S18}$$

Here we can see that x_R, a_0, and h_0 are all constants. Hence, we can use the product of ASP and $k^{1.2}$ to examine the behavior of consumption rate (Fig. S5). Firstly, for $= \frac{1}{1+k^\gamma}$, let $f(k) = A \cdot k^{1.2} = \frac{k^{1.2}}{1+k^2}$ ($\gamma = 2$). Then $f' = \frac{k^{0.2} - k^{2.2}}{(1+k^2)^2}$, so for $k \in [0, \infty]$, there is only one maximum at $k = 1$ (Fig. S5b). Then by definition, $f(k)$ is a unimodal function for $k \in [0, \infty]$. Similarly, for $ASP = \hat{A} = \exp\left[-\frac{(k-k_{pk})^2}{2\sigma^2}\right]$, let $g(k) = \hat{A} \cdot k^{1.2} = k^{1.2} \exp\left[-\frac{(k-1)^2}{2}\right]$ ($k_{pk} = 1, \& \, \sigma^2 = 1$). Then $g' = \exp\left[-\frac{(k-k_{pk})^2}{2\sigma^2}\right] (1.2k^{0.2} - k^{2.2} + k^{1.2})$, so for $k \in [0, \infty]$, there is only one maximum at $k = \frac{1+\sqrt{5.8}}{2} \approx 1.7$ (Fig. S5b). Hence by definition $g(k)$ is also a unimodal function.

Next, we compare both ASP models in the limits of very small (k ≪ 1) and large (k ≫ 1 + σ) size-ratios. Here, we assume an intermediate value for the optimal size-ratio, then we further assume that the variance in ASP is significantly larger than the optimal size-ratio. More specifically, for $k_{pk} = 1, \gamma = 2, \sigma \gg 1, and \; k \ll 1$

$$ASP \cdot k^{1.2} = \begin{cases} k^{1.2}(1+k^2)^{-1} \sim (1-k^2)k^{1.2} = k^{1.2} - k^{3.2} \sim k^{1.2} \\ k^{1.2} \exp\left(-\frac{(k-1)^2}{\sigma^2}\right) \sim \left(1 - \frac{(k-1)^2}{\sigma^2}\right) k^{1.2} = k^{1.2}\left(1 - \frac{1}{\sigma^2}\right) + \frac{2k^{2.2}}{\sigma^2} - \frac{k^{3.2}}{\sigma^2} \sim k^{1.2} \end{cases} \tag{S19}$$

If we relax the idea of optimum size-ratio for attack success probability, we can see that large σ gives the same asymptotic form for both ASP models and for $k \gg 1 + \sigma$

$$ASP \cdot k^{1.2} = \begin{cases} k^{1.2}(1+k^2)^{-1} = k^{-0.8} \longrightarrow 0 \\ k^{1.2} \exp\left(-\frac{(k-1)^2}{\sigma^2}\right) \longrightarrow 0 \end{cases} \tag{S20}$$

Notice that although the two models approach 0 at different rates, they both approach 0 asymptotically. Finally, for intermediate values of $ASP \cdot k^{1.2}$, the term $\frac{1}{a_0 ASP \cdot k^{1.2}}$ will be relatively small compared to large h_0 values (Equation (S18)) Therefore, it is sufficient to say that even though the two ASP models above are quantitatively different across all of function space, the consumption rate behaves very similarly qualitatively under both models in these three limits. Furthermore, monotonic and Gaussian-like ASP models also produce only minor differences in predicted coexistence regions (Fig. S6).

Taken together, our analysis shows that both ASP models exhibit a qualitatively similar, unimodal relationship between size ratio and consumption rate. Furthermore, both ASP models show asymptotically

similar behavior for small (k ≪ 1) and large (k ≫ 1 + σ) size ratios. For the intermediate size-ratios, consumption rate is similar in both models for sufficiently large values of handling times (h_0).

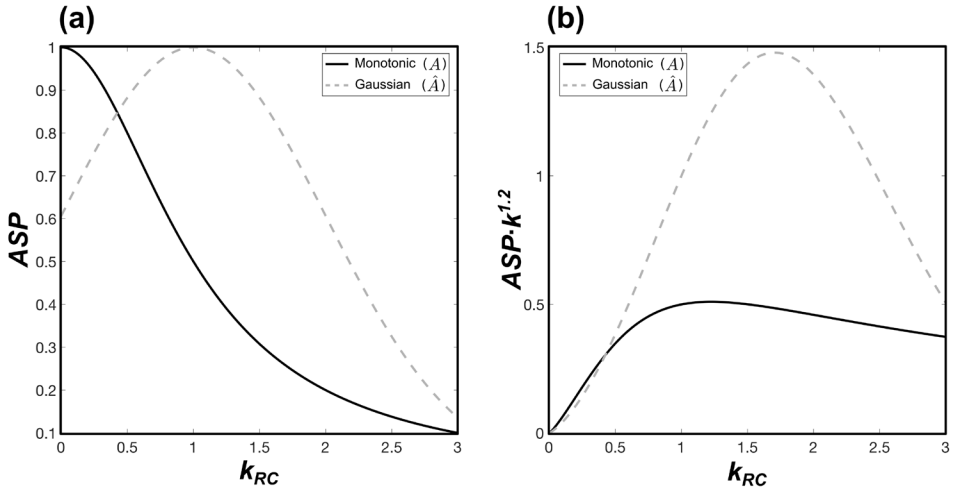

Figure S5. Comparing the influence of monotonic and Gaussian ASP models on consumption rate. (a) ASP as a function of size-ratio (k) for both models. (b) The key element of consumption rate (ASP × $k^{1.2}$) across size-ratios.

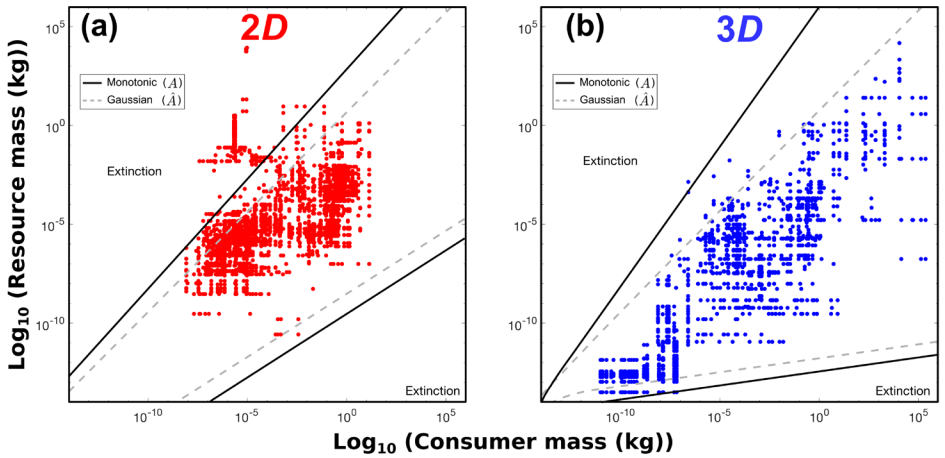

Figure S6. Comparing the influence of monotonic and Gaussian ASP models on consumer-resource coexistence regions in 2D (a) and 3D (b).

Effect of geometric mean resource size on size and size-ratio distributions

In order to account for non-independent size-ratios, we re-analyzed the empirical community data for differences between 2*D* and 3*D* size-ratios after collapsing all the links of a single consumer to a single size ratio by taking the geometric average of the sizes of all its resources. By comparing this analysis (Table S4) with the main analysis (main text Table 1), we see that the the main conclusions about differences in the central tendencies of size-ratio distributions in 2*D* versus 3*D* remain qualitatively unchanged.

Table S4. Differences between 2*D* and 3*D* size-ratio distributions using the geometric mean of all resource sizes of each consumer. The Median $\log_{10}$(Size-ratio) column shows observed medians of $\log_{10}$ transformed size-ratios, and their observed and predicted (in parentheses) difference in medians (3*D*–2*D*). All observed differences are significantly different from 0 ($p < 0.05$; flagged with an asterisk) based upon a randomization test (see main text). Note that although median 2*D* and 3*D* size-ratios are significantly different in most communites, median 2*D* and 3*D* consumer and resource sizes are not ($p > 0.05$; Wilcoxon–Mann–Whitney test with shared taxa removed). The 2*D* / 3*D* overlap column shows proportion of consumers in each community feeding on both 2*D* and 3*D* resources (Jaccard index) (Con), and proportion of resources exploited by both 2*D* and 3*D* consumers (Res). If such an overlap exists, the total number of taxa (Taxa-All) within a community will be smaller than the sum of 2*D* and 3*D* taxa.

Community	Median $\log_{10}$(Size-ratio)			Median $\log_{10}$(Size)		Taxa			Interactions			2*D* / 3*D* overlap	
	2*D*	3*D*	3*D*–2*D*	2*D*	3*D*	All	2*D*	3*D*	All	2*D*	3*D*	Con	Res
All communities	-0.23	-3.57	-3.34* (-2.28)	-4.79	-4.05	785	539	339	814	500	314	0.09	0.59
Eastern Weddell Sea	-0.85	-3.92	-3.07* (-2.03)	-2.78	-2.51	276	82	234	286	70	216	0.11	0.58
Estero de Punta Banda	-2.88	-4.48	-1.60* (-1.00)	-2.48	-2.73	105	97	41	102	69	33	0.34	0.24
Grand Cariçaie Marsh	-0.23	-1.18	-0.95 (-1.20)	-5.55	-5.44	75	54	24	52	36	16	0.00	0.13
Scotch Broom	-0.20	-0.91	-0.71 (-1.02)	-5.44	-5.28	159	156	6	149	146	3	0.00	0.30
Skipwith Pond	-0.76	-2.92	-2.16* (-0.39)	-4.69	-4.55	34	31	19	32	18	14	0.78	0.13
Broadstone Stream	-0.98	–	–	-6.71	–	16	16	0	9	9	0	–	–
Gearagh Woodland	-0.18	–	–	-5.56	–	113	113	0	99	99	0	–	–
UK Grasslands	0.37	–	–	-5.40	–	61	61	0	53	53	0	–	–
Tuesday Lake	–	-3.07	–	–	-10.9	47	0	47	32	0	32	–	–

References

Aljetlawi, A. A., Sparrevik, E. & Leonardsson, K. (2004). Prey-predator size-dependent functional response: derivation and rescaling to the real world. *J. Anim. Ecol.* **73**, 239–252.

Bailey, P. C. E. (2010). The Feeding Behaviour of a Sit and Wait Predator Ranatra dispar (Heteroptera: Nepidae): The Effect of Prey Density and Age Structure on the Number of Prey Eaten. *Ethology* **72**, 277–286.

Brose, U., Ehnes, R. B., Rall, B. C., Vucic-Pestic, O., Berlow, E. L. & Scheu, S. (2008). Foraging theory predicts predator-prey energy fluxes. *J. Anim. Ecol.* **77**, 1072–8.

Brown, J. H., Gillooly, J. F., Allen, A. P., Savage, V. M. & West, G. B. (2004). Toward a metabolic theory of ecology. *Ecology* **85**, 1771–1789.

Dell, A. I., Pawar, S. & Savage, V. M. (2011). Systematic variation in the temperature dependence of physiological and ecological traits. *Proc. Natl. Acad. Sci. U. S. A.* **108**, 10591–10596.

Dell, A. I., Pawar, S. & Savage, V. M. (2013). The thermal dependence of biological traits. *Ecology* **94**, 1205.

Dierckens, K., Sarma, S., Mertens, J. & Dumont, H. (1995). Feeding the fairy shrimp Streptocephalus (Anostraca-Crustacea) with the rotifer Anuraeopsis. *Hydrobiologia* **308**, 29–33.
Fantinou, A. A., Perdikis, D. C., Labropoulos, P. D. & Maselou, D. A. (2009). Preference and consumption of Macrolophus pygmaeus preying on mixed instar assemblages of Myzus persicae. *Biol. Control* **51**, 76–80.
Galarowicz, T. & Wahl, D. (2005). Foraging by a young-of-the-year piscivore: the role of predator size, prey type, and density. *Can. J. Fish. Aquat. Sci.* **2342**, 2330–2342.
Gergs, A. & Ratte, H. T. (2009). Predicting functional response and size selectivity of juvenile Notonecta maculata foraging on Daphnia magna. *Ecol. Modell.* **220**, 3331–3341.
Hansen, B. & Ockelmann, K. (1991). Feeding behaviour in larvae of the opisthobranch Philine aperta I. Growth and functional response at different developmental stages. *Mar. Biol.* **111**, 255–261.
Jansen, P. A., Finstad, A. G. & Langeland, A. (2003). Size-scaling of zooplankton foraging in Arctic charr. *J. Fish Biol.* **62**, 860–870.
Lang, B., Ehnes, R. B., Brose, U., and Rall, B. C. (2017). Temperature and consumer type dependencies of energy flows in natural communities. Oikos **126**, 1717–1725.
Miller, T., Crowder, L. B., Rice, J. A. & Birskowski, F. P. (1992). Body Size and the Ontogeny of the Functional Response in Fishes.
Nagy, K. A. (2005). Field Metabolic Rate and Body Size. Journal of Experimental Biology **208** (9): 1621–1625.
Pawar, S., Dell, A. I. A. & Savage, V. M. V. (2012). Dimensionality of consumer search space drives trophic interaction strengths. *Nature* **486**, 485–489.
Pawar, S., Dell, A. I., and Savage, V. M. (2015). From Metabolic Constraints on Individuals to the Dynamics of Ecosystems, in Aquatic Functional Biodiversity, eds. A. Belgrano, G. Woodward, and U. Jacob. San Diego: Academic Press.
Persson, L., Leonardsson, K., de Roos, a M., Gyllenberg, M. & Christensen, B. (1998). Ontogenetic scaling of foraging rates and the dynamics of a size-structured consumer-resource model. *Theor. Popul. Biol.* **54**, 270–293.
Peters, R. (1986). The ecological implications of body size. Cambridge: Cambridge University Press.
Savage, V. M., Gilloly, J. F., Brown, J. H., Charnov, E. L., Gillooly, J. F. & West, G. B. 2004 Effects of body size and temperature on population growth. *Am. Nat.* **163**, 429–41.
Uye, S. & Kayano, Y. (1994). Predatory feeding behavior of Tortanus (Copepoda: Calanoida): life-stage differences and the predation impact on small planktonic crustaceans. *J. Crustac. Biol.* **14**, 473–483.
Vucic-Pestic, O., Rall, B. C., Kalinkat, G. & Brose, U. (2010). Allometric functional response model: body masses constrain interaction strengths. *J. Anim. Ecol.* **79**, 249–56.
Walne, P. & Dean, G. (1972). Experiments on predation by the shore crab, Carcinus maenas L., on Mytilus and Mercenaria. *J. du Cons.* **34**, 190–199.
Warton, D. I., Wright, I. J., Falster, D. S. & Westoby, M. (2006). Bivariate line-fitting methods for allometry. *Biol. Rev. Camb. Philos. Soc.* **81**, 259–91.
Weitz, J. S. & Levin, S. A. (2006). Size and scaling of predator-prey dynamics. *Ecol. Lett.* **9**, 548–57.
Yodzis, P. & Innes, S. (1992). Body size and consumer-resource dynamics. Am. Nat. 139, 1151–1175.